Infinite Rotational Motion Generation and Analysis of a Spherical Parallel Manipulator with Coaxial Input Axes ⋆,⋆⋆

Iliyas Tursynbek[a], Almas Shintemirov[a,*]

[a]*Department of Robotics and Mechatronics, Nazarbayev University, Nur-Sultan, Kazakhstan*

Abstract

This paper presents a novel framework for the analysis of a 3-RRR spherical parallel manipulator with coaxial input axes (coaxial SPM) with the focus on its infinite rotational motion capabilities and its effects on the manipulator's characteristics. The framework consists of three phases. At first, an approach for obtaining unique solutions of forward and inverse kinematics problems is introduced for setting up univocal relation between coaxial SPM's input joint positions and orientation of its end-effector. At the second phase, a method for generating infinite rotational motions of an end-effector is formulated. The third phase outlines numerical computation procedures of the coaxial SPM's workspaces in the joint and Cartesian spaces, excluding singularity configurations and mechanical collisions of SPM's links during infinite rotational motion. A 3D design model and an experimental prototype of the coaxial SPM is presented and utilized for numerical analysis and experimental verification of the presented framework supplemented by an accompanying video demonstration.

Keywords:
spherical parallel manipulator, kinematic analysis, infinite rotational motion, workspace analysis, joint-space trajectory generation, motion planning

1. Introduction

Parallel manipulators are under constant attention of academia and industry due to their theoretical advantage over serial manipulators regarding their increased positioning and orienting accuracy, mechanical rigidity and performance in high dynamic motions. However, such manipulators need a very detailed research and analysis conducted on them before they can find their use in industry [1–5]. A class of parallel manipulators known as spherical parallel manipulators (SPMs) is able to provide a three degrees-of-freedom (3-DOF) pure rotational motion. They are considered to be an alternative to traditional robotic wrists utilizing serial arrangement of their links [6] and can serve as spherical motion generators [7]. Their application spans from manufacturing [8] and motion control platforms [9] to medicine [10, 11] and rehabilitation [12, 13].

Among numerous types of 3-DOF SPMs that were synthesized [14–18], the 3-RRR type SPMs, i.e., with three revolute joints (R) at each of the three parallel chains, are the most studied in detail (hereafter - general SPM). The early research works by Gosselin *et al.* [19–21] set the foundations of kinematic design and analysis of 3-RRR SPMs. These works introduced the notation and approaches to solve forward and inverse kinematics of general SPMs. It was also validated there that multiple solutions to both forward and inverse kinematic problems exist. Despite the substantial theoretical research conducted on this topic, only a few SPMs were designed and built in the real world for experimental analysis and practical applications [22, 23].

The above-mentioned works primarily focus on SPMs with a limited range of motion of the DOF corresponding to an end-effector's rotation around its normal vector. For example, the *Agile Eye*

⋆This paper was accepted for publication in Mechatronics. DOI 10.1016/j.mechatronics.2021.102625

⋆⋆This research was supported by the Kazakhstan Ministry of Education and Science (project IRN AP08052091).

*Corresponding author

Email addresses: iliyas.tursynbek@nu.edu.kz (Iliyas Tursynbek), ashintemirov@nu.edu.kz (Almas Shintemirov)

[9] prototype is capable of only $\pm 30^\circ$ of the end-effector's twist. This limitation does not allow such SPMs to be used to the fullest extent as active ball joints or orientation platforms for machining tools [24] since these applications often require complete 360° or infinite rotational motion. A special case of the general SPM with a collinear (coaxial) arrangement of its input axes (hereafter - coaxial SPM) does not have this limitation, making it a potential candidate for such applications.

Coaxial SPM's kinematic structure shown in Fig. 1b was initially presented in [25], where several serial and parallel wrist joints were assessed for their kinematic and static performances. The optimal design of such wrist joints was considered from the reduced singularity and uniform velocity behavior viewpoints. It was reported that for specific geometrical parameters of the coaxial SPM's links, the velocity ratio is much more isotropic and less dependent on the SPM's configuration. One of the advantages of the proposed manipulator in [25] is that it has no singularities inside the workspace, only on the boundaries, compared to the serial counterparts. This SPM architecture was further studied in [26] by Gosselin *et al.*, where it was shown that such SPMs have eight solutions for the forward kinematic problem similar to the general SPMs. Subsequently, the coaxial SPM was used to design marine propulsors [27, 28] and a robotic link mechanism [29]. In these works, actuators are fixed and located on the base of the designed devices, which allows remote actuation of the mechanisms and, in general, decreases manipulators' inertia. Alternative mechanical design of the coaxial SPM, with sliding actuators was presented in [30, 31], which improves stiffness of the manipulator's legs due to the presence of a circular guide. The subsequent works [8, 32] focus on design optimization of this proposed coaxial SPM's design from the kinematics and dynamics viewpoints with no reported experimental demonstration on the physical coaxial SPM's prototype. SPMs with infinite rotation of the end-effector around its normal vector were also accomplished using different joints arrangement, such as in [33] were authors analyzed a 3(RSS)-S fully spherical robot. Other theoretical mechanical designs of the coaxial SPMs were based on kinematically asymmetrical SPM, i.e., with different combination of joints in each link, were also reported [34–36]. In general, analysis of such mechanisms is more complex than that of symmetrical SPMs, which demands further efforts for their physical realization.

Despite the considerable interest in the coaxial SPMs, the above reviewed works focus primarily on mechanical design optimization, kinematic and dynamic analyses of the proposed SPM designs without considering the effect of the infinite rotational motion on the manipulator's workspace and the ways to achieve such motions. To the authors' belief, no research works were publicly reported to the date, outlining theoretical foundations for the generation of infinite rotational motions of the coaxial SPM with the corresponding joint space and Cartesian workspace analyses required for practical applications of such manipulators. This paper addresses this knowledge gap and presents a novel framework for generating infinite rotational motions and further kinematic analysis of the SPM with coaxial input axes. It consists of three phases. The first phase, outlined in Section 2, presents the approach for obtaining unique solutions to the forward and inverse kinematic problems for univocal relation of the coaxial SPM's input joint positions to the orientation of its end-effector and vice versa. At the second phase, a method for generating infinite rotational motions of the manipulator's end-effector is formulated as detailed in Section 3. The last phase is presented in Section 4. It outlines singularity and link collision detection procedures for numerical computation of the coaxial SPM's configuration space and the Cartesian workspace, considering infinite rotational motion feature of the manipulator. A 3D CAD model and an experimental prototype of the coaxial SPM are presented in Section 5 and utilized for numerical analysis and experimental verification of the presented framework in Section 6, supplemented by an accompanying video demonstration.

The approaches and numerical computations presented in this paper are a systematic revision and extension of the preliminary results reported in the authors' conference works [37, 38]. A combined framework for generating infinite rotational motions of a coaxial SPM and study of their effects is the main contribution of this paper. In contrast to the author's earlier works [39, 40], a numerical approach presented there for computing the unique forward and inverse kinematics of a coaxial SPM was revised for a better alignment of analytical formulations with the pioneering work on SPM [21] and augmentation by a novel expression for automated definition of an initial guess vector. The second contribution of this paper is the overall ex-

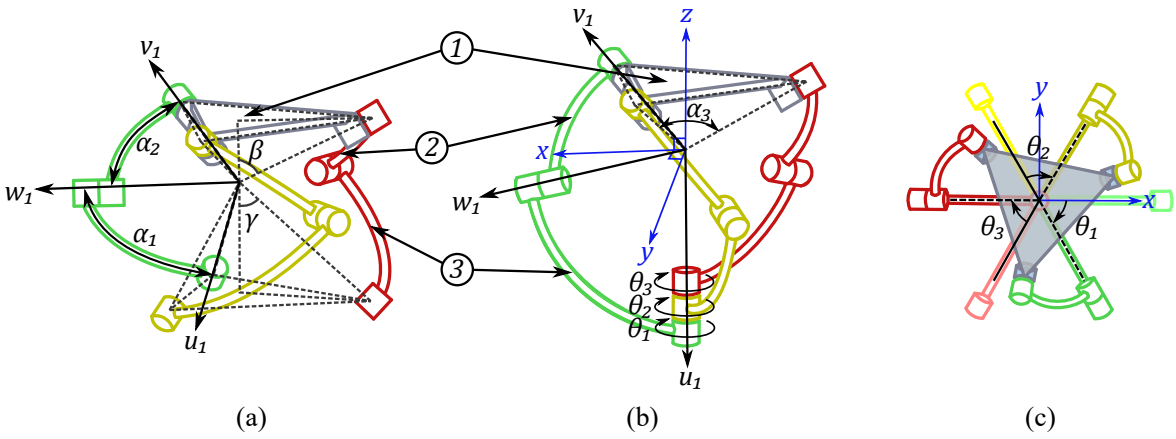

Figure 1: SPM's kinematic models: (a) general SPM, where (1) - mobile platform, (2) - distal link, (3) - proximal link; (b) coaxial SPM; (c) positive direction of the input joint positions with respect to the home configuration (shown only with the proximal links).

perimental implementation and verification of the proposed framework on an experimental prototype of the coaxial SPM, thus demonstrating its practical applicability to design SPM-based mechanisms with infinite rotational motion capabilities.

2. Kinematic Analysis

Kinematic analysis, configuration space (joint space) and Cartesian workspace characterizations are important first stages in the design of robotic manipulators. These procedures are more complicated for parallel manipulators comparing to serial ones. In the case of the coaxial SPM and 3-DOF 3-RRR SPMs in general, as was mentioned previously, there exist multiple solutions to its forward and inverse kinematic problems [20]. Analytical solution to the inverse kinematic problem of 3-RRR SPMs was derived in [19, 41]. Whereas, the closed-form solution to the forward kinematic problem of 3-RRR SPMs using polynomial approach was proposed later in [21], where the authors derived a polynomial of degree 8, and demonstrated that this polynomial is minimal and solving it provides 8 real solutions to the SPM forward kinematic problem. Later, a different approach based on semigraphical method was proposed in [42]. This method is based on the input–output equations of spherical four-bar linkages and requires solving derived trigonometric equations semigraphically to obtain the joint variables for the determination of the moving platform orientation. Both methods, i.e., polynomial and semigraphical, involve solving complex nonlinear equations that may be computationally heavy for implementation of real-time control of SPMs. Therefore, special architectures of SPMs resulting in simplified kinematic equations were proposed in [26, 43], that are employed for achieving real-time control of a SPM with special architecture (*Agile Eye*) in [9]. It is also a common practice to add extra sensors to obtain redundant data resulting in simplified closed-form solutions [44, 45] or to utilize various numerical methods to solve forward kinematic problem of parallel manipulators [46]. Moreover, for control applications it is also required to be able to select a single solution from the several ones, such that it always corresponds to a specific assembly of SPM. In this regard, a numerical approach for obtaining unique solutions, corresponding to a working or assembly mode of a real SPM, was proposed in [39]. Identification of one unique solution for the forward and inverse kinematics is required for orientation and/or stabilization control and motion planning of a device based on SPM architecture [47, 48]. This approach was subsequently utilized to develop offline motion planning and real-time orientation control frameworks for this type of SPMs using convex optimization techniques that were experimentally verified on the *Agile Wrist* SPM prototype in [40, 49]. The author's preliminary works, [37] and [38], report extension of the results from [39, 40] to a coaxial SPM model case study and discuss its unique forward and inverse kinematics, assembly and working modes, generation and sim-

ulation modeling of infinite rotational motion, respectively. This approach was also tested and verified via external control of a simulation model of coaxial SPM in CoppeliaSim (formerly known as V-REP) [50] open-access virtual robotic simulator in [51]. Parallel manipulators can be physically simulated and controlled in CoppeliaSim directly or remotely from external environments such as MATLAB. Position data about manipulator's joints, obtained directly in CoppeliaSim, were used for verification analysis of the proposed approach in [51]. As a result, it was concluded that the numerically derived unique solutions to the SPM forward kinematic problem coincide with the simulated orientation of the physical SPM model (Figure 6 in [51]).

Being a special case of the general SPM, kinematic analysis of the coaxial SPM is based on the same fundamentals as in [20, 21, 42, 52]. This section briefly introduces fundamentals of SPM's kinematics, as well as a revised approach for obtaining unique kinematic solutions of the coaxial SPM, initially presented by the authors in [37].

2.1. Kinematic Model

A geometric model of the general 3-RRR SPM is represented as two triangular pyramid-shaped platforms, mounted on top of each other and sharing a single vertex as shown with dotted lines in Fig. 1a. The lower platform is a (stationary) *base* and is defined by angle γ. The upper platform is a *mobile platform*, which undergoes 3-DOF spherical motion, and is defined by angle β. In the special case of the coaxial SPM, the lower platform is degenerated to a single line by coaxial placement of the base joints, i.e. *input joints*, as demonstrated in Fig. 1b. In this arrangement of the base joints, angle $\gamma = 0^\circ$. Such special arrangement of the input joints allows infinite rotational motion of the SPM's mobile platform.

Three equally spaced parallel chains connect the mobile platform to the base. They are enumerated as $i = 1, 2, 3$ in the counter-clockwise direction. Each chain consists of two curved *links*: *proximal* and *distal*. The curvature of the proximal link is defined by angle α_1, whereas that of the distal link is defined by angle α_2. Each parallel chain has three joints, the axes of which intersect at the common point known as the *center of rotation*. Those axes are defined by the unit vectors $\mathbf{u}_i$, $\mathbf{w}_i$, and $\mathbf{v}_i$, respectively from the base to the mobile platform, α_3 denotes an angle between any two unit vectors $\mathbf{v}_i$.

To define location of the mobile platform, a stationary coordinate system needs to be set up. The right-handed coordinate system is placed at the center of rotation as shown in Fig. 1b. The z-axis is directed upwards, whereas the x-axis is orthogonal to the z-axis and is pointing towards the intermediate joint of the first parallel chain at the home configuration. The right-hand rule is used to determine the y-axis. At the *home configuration*, proximal links are located 120° from each other, making the mobile platform horizontal with its normal vector coincident with the positive z-axis.

The inputs to the coaxial SPM are provided by actuating proximal links via base joints. Those input joints positions are measured in the clockwise direction from the central symmetry planes of the proximal links at the home configuration till the same planes at the resultant location as illustrated in Fig. 1c. The input joints positions are represented by vector $\boldsymbol{\theta} \triangleq \begin{bmatrix}\theta_1, & \theta_2, & \theta_3\end{bmatrix}^T$, and at the home configuration it is set to $\boldsymbol{\theta} = \begin{bmatrix}0, & 0, & 0\end{bmatrix}^T$.

Following the earlier definition of the coordinate system, the base joints' unit vectors $\mathbf{u}_i$, $i = 1, 2, 3$, are expressed as:

$$\mathbf{u}_i = \begin{bmatrix} 0 \\ 0 \\ -1 \end{bmatrix}. \tag{1}$$

The intermediate joints' unit vectors $\mathbf{w}_i$, $i = 1, 2, 3$, are defined as follows:

$$\mathbf{w}_i = \begin{bmatrix} \cos(\eta_i - \theta_i)\sin\alpha_1 \\ \sin(\eta_i - \theta_i)\sin\alpha_1 \\ -\cos\alpha_1 \end{bmatrix}, \tag{2}$$

where $\eta_i = 2(i-1)\pi/3$, $i = 1, 2, 3$.

The orientation of the coaxial SPM is defined by the the unit vectors of the mobile platform's joints $\mathbf{v}_i$, $i = 1, 2, 3$.

2.2. Forward Kinematics

In the case of the coaxial SPM, the forward kinematics is used to describe the orientation of the mobile platform in terms of the unit vectors $\mathbf{v}_i$, $i = 1, 2, 3$, given the input joint positions vector $\boldsymbol{\theta}$. To compute these unit vectors, nine independent equations are derived from geometric constraints of SPMs [42]:

$$\begin{cases} \mathbf{w}_i \cdot \mathbf{v}_i = \cos\alpha_2, & i = 1, 2, 3, \\ \mathbf{v}_i \cdot \mathbf{v}_j = \cos\alpha_3, & i, j = 1, 2, 3, \quad i \neq j, \\ \|\mathbf{v}_i\| = 1, \end{cases} \tag{3}$$

where $\alpha_3 = 2\sin^{-1}\left(\sin\beta\cos\frac{\pi}{6}\right)$ is the angle between axes of the ith and jth mobile platform joints (Fig. 1b), and $\|\cdot\|$ is the Euclidean norm.

The system of equations (3) provides multiple solutions and can be solved for $\mathbf{v}_i$'s numerically. In this work, the trust-region numerical optimization method for solving nonlinear programming problems is employed [53]. In MATLAB, it is implemented as `fsolve` function with a default `trust-region-dogleg` algorithm and an initial guess vector $\boldsymbol{x}_0$. In case of Python, it is implemented with `scipy.optimize.minimize` method with `method = 'dogleg'` parameter and the same initial guess vector $\boldsymbol{x}_0$ as in MATLAB's case. This vector's values are the guesses of x, y, and z components of the unit vectors $\mathbf{v}_i$, $i = 1, 2, 3$, represented as follows:

$$\boldsymbol{x}_0 = \left[v_{1x}, v_{1y}, v_{1z}, v_{2x}, v_{2y}, v_{2z}, v_{3x}, v_{3y}, v_{3z}\right]^T. \quad (4)$$

In this paper, the *l-l-l* assembly mode [37] is chosen for the analysis, meaning that all distal links are located to the left of the central symmetry plane of the respective proximal links. By the definition of this assembly mode, it is expected that the unit vectors $\mathbf{v}_i$, $i = 1, 2, 3$, are always further in the positive direction of link rotations (clockwise), thus the guess vector is chosen as the positive shifted instance of the unit vectors $\mathbf{w}_i$, $i = 1, 2, 3$, and pointing in the same z direction as at the home configuration. An example of such shift of the unit vectors $\mathbf{w}_i$, $i = 1, 2, 3$, could be a 10° rotation around the z-axis, expressed using the Rodrigues' rotation formula [54] as follows:

$$\begin{aligned}\mathbf{w}_{i,rot} = \mathbf{w}_i\cos 10^\circ + \left(\mathbf{w}_i \times \begin{bmatrix}0\\0\\1\end{bmatrix}\right)\sin 10^\circ + \\ + \begin{bmatrix}0\\0\\1\end{bmatrix}\left(\begin{bmatrix}0\\0\\1\end{bmatrix}\cdot \mathbf{w}_i\right)\left(1-\cos 10^\circ\right), \quad i = 1, 2, 3.\end{aligned} \quad (5)$$

The resultant guess vector is then formulated as follows:

$$\begin{aligned}\boldsymbol{x}_0 = [\, & w_{1x,rot}, w_{1y,rot}, -w_{1z,rot}, \\ & w_{2x,rot}, w_{2y,rot}, -w_{2z,rot}, \\ & w_{3x,rot}, w_{3y,rot}, -w_{3z,rot}]^T.\end{aligned} \quad (6)$$

The z components of the guess vector, i.e. $w_{1z,rot}$, $w_{2z,rot}$, and $w_{3z,rot}$, are negated as the unit vectors $\mathbf{w}_i$, $i = 1, 2, 3$, have these components in the negative z direction (for cases when $\alpha_1 < 90^\circ$), but typically the unit vectors $\mathbf{v}_i$ $i = 1, 2, 3$, have z components pointing in the positive direction. Selecting this guess vector allows to obtain a unique solution of the forward kinematics problem corresponding to the *l-l-l* assembly mode. Note that for the alternative symmetrical *r-r-r* assembly mode, (5) will have -10° shift (negative direction of rotation).

The computation process of a unique forward kinematics solution is summarized in the updated Algorithm 1. It was initially formulated and experimentally verified by the authors in [37]. Here, an additional step for calculating $\mathbf{w}_i$ is introduced for obtaining a new guess vector.

Algorithm 1: Obtaining a unique solution of the forward kinematics problem of a coaxial SPM

Input: $\boldsymbol{\theta}$, α_1, α_2, β, $\boldsymbol{x}_0$, η_i, $i = 1, 2, 3$
Output: Unique unit vectors $\mathbf{v}_i$, $i = 1, 2, 3$

Calculate $\alpha_3 = 2\sin^{-1}\left(\sin\beta\cos\frac{\pi}{6}\right)$;
for $i \leftarrow 1$ **to** 3 **do**
  Calculate $\mathbf{w}_i$ using (2) given $\boldsymbol{\theta}$;
  Calculate $\mathbf{w}_{i,rot}$ using (5);
Calculate initial guess vector $\boldsymbol{x}_0$ using (6);
Calculate $\mathbf{v}_i$, $i = 1, 2, 3$, by solving the system of equations (3) numerically, given $\mathbf{w}_i$, $i = 1, 2, 3$, with initial guess vector $\boldsymbol{x}_0$;
return $\boldsymbol{v}_i$, $i = 1, 2, 3$

2.3. Inverse Kinematics

In the case of the coaxial SPM, the inverse kinematics is used to compute the input joint positions vector $\boldsymbol{\theta}$ that can be applied to bring the mobile platform to a specific orientation described by the unit vectors $\mathbf{v}_i$, $i = 1, 2, 3$. Three uncoupled equations used to compute each of input joint positions θ_i, $i = 1, 2, 3$, are formulated as follows [20]:

$$A_i T_i^2 + 2\,B_i T_i + C_i = 0, \quad i = 1, 2, 3, \quad (7)$$

with

$$T_i = \tan\left(\frac{\theta_i}{2}\right). \quad (8)$$

These equations are derived from the first equation from the system of equations (3), and have

coefficients A_i, B_i, and C_i formulated as follows:

$$\begin{aligned} A_i = & -\cos\eta_i \sin\alpha_1 v_{ix} - \sin\eta_i \sin\alpha_1 v_{iy} - \\ & -\cos\alpha_1 v_{iz} - \cos\alpha_2; \\ B_i = & \sin\eta_i \sin\alpha_1 v_{ix} - \cos\eta_i \sin\alpha_1 v_{iy}; \\ C_i = & \cos\eta_i \sin\alpha_1 v_{ix} + \sin\eta_i \sin\alpha_1 v_{iy} - \\ & -\cos\alpha_1 v_{iz} - \cos\alpha_2, \end{aligned} \tag{9}$$

where v_{ix}, v_{iy}, and v_{iz} are components of the unit vectors $\mathbf{v}_i$, $i = 1, 2, 3$.

Compared to the numerical computation of the forward kinematics solutions, the inverse kinematics solutions are solved analytically. Equations (7) are decoupled quadratic equations for each input joint position θ_i, $i = 1, 2, 3$ with two roots for each T_i. This results in total of eight combinations of possible solutions for the input joint positions, representing eight *working modes*. To compute the solution corresponding to the coaxial SPM operating in the *l-l-l* working mode as discussed in [37, 49], it is necessary to select the solution that corresponds to the roots with added square root of the discriminant (the definition of the positive direction of rotation). On the other hand, the combination corresponding to the roots with subtracted square root of the discriminant presents the solution for the *r-r-r* working mode.

Similarly to the forward kinematics, the updated Algorithm 2 for obtaining unique solutions of the inverse kinematics problem is given below. It was initially formulated and tested by the authors in [37]. However, compared to the previous version of the Algorithm, the coefficients A_i, B_i, and C_i are calculated differently. The direction of legs indexing (counter-clockwise), the definition of the positive direction of rotation (clockwise, right-hand rule applied on vectors $\mathbf{u}_i$, $i = 1, 2, 3$), and the alignment of the SPM's home configuration with the fixed coordinates system have been modified from that of [37]. This has been done in order to comply with the pioneering works of Gosselin *et al.* [21] and to preserve nomenclature and definition consistency. Introduction of these changes resulted in modification of (9) for calculating coefficients A_i, B_i, C_i.

3. Generation of Infinite Rotational Motions

Ability to generate infinite rotational motions of the mobile platform around its normal vector, as shown in Fig. 2, is one of the distinctive features of the coaxial SPM that makes it different from the other special kinematic architectures of the 3-RRR SPMs such as the SPM with coplanar actuators [20] or the *Agile Eye* [9]. Rotational motion of the coaxial SPM requires generation of the sequence of input joint positions $\boldsymbol{\theta}_{traj}$, i.e., actuator motion trajectories. This section presents an approach of trajectory generation for infinite rotational motions of the coaxial SPM.

Algorithm 2: Obtaining a unique solution of the inverse kinematics problem of a coaxial SPM

Input: $\mathbf{v}_i$, $i = 1, 2, 3$, α_1, α_2, η_i
Output: Input joint positions vector $\boldsymbol{\theta}$

for $i \leftarrow 1$ **to** 3 **do**
  Calculate A_i, B_i, C_i using (9) given $\mathbf{v}_i$;
  Solve equation (7) for T_i;
  Find θ_i using equation (8) and select solution coming from the root with added or subtracted square root of the discriminant for *l-l-l* or *r-r-r* working mode, respectively;
return θ_i, $i = 1, 2, 3$

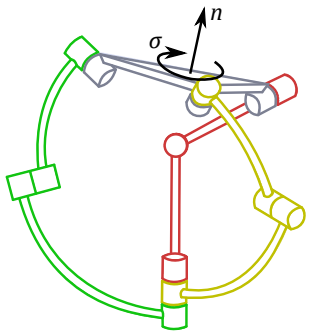

Figure 2: Rotation of the coaxial SPM mobile platform around its normal vector $\mathbf{n}$ by angle σ.

In the proposed framework, the orientation of the coaxial SPM's mobile platform is defined by the unit vectors $\mathbf{v}_i$, $i = 1, 2, 3$. Hence, the rotational motion of the SPM's mobile platform around its normal vector $\mathbf{n}$ can be interpreted as the rotation of the unit vectors $\mathbf{v}_i$, $i = 1, 2, 3$, around the same vector $\mathbf{n}$, which is computed as:

$$\begin{cases} \mathbf{n} = \dfrac{\mathbf{v}_1 + \mathbf{v}_2 + \mathbf{v}_3}{\|\mathbf{v}_1 + \mathbf{v}_2 + \mathbf{v}_3\|}, & \forall\, \beta \neq 90°, \\ \mathbf{n} = \dfrac{\mathbf{v}_1 \times \mathbf{v}_2}{\|\mathbf{v}_1 \times \mathbf{v}_2\|}, & \forall\, \beta = 90°. \end{cases} \tag{10}$$

The instantaneous orientation of the SPM's mo-

bile platform during the rotational motion is defined by the unit vectors $\mathbf{v}_{i,rot}$, $i = 1, 2, 3$, and is computed using the Rodrigues' rotation formula [54]:

$$\begin{aligned}\mathbf{v}_{i,rot} = &\mathbf{v}_i \cos\sigma + (\mathbf{v}_i \times \mathbf{n}) \sin\sigma + \\ &+ \mathbf{n}(\mathbf{n} \cdot \mathbf{v}_i)(1 - \cos\sigma), \quad i = 1, 2, 3,\end{aligned} \tag{11}$$

where σ is a rotation angle of the SPM's platform measured from the starting configuration till the final rotational instance as shown in Fig. 2.

In order to generate trajectories for infinite rotational motion, a single full 360° rotation of the SPM's mobile platform is sampled into a sequence of S instances with the rotation angles as:

$$\boldsymbol{\sigma} = \{\sigma_1,\ \sigma_2,\ \ldots\ \sigma_S\}. \tag{12}$$

A uniform sampling interval of the rotation is employed for the simplicity of the numerical analysis, i.e., $\delta_\sigma \triangleq \sigma_{j+1} - \sigma_j$, $j = 1, 2, \ldots S-1$, is constant.

The procedure for obtaining a unique inverse kinematics solution, i.e., Algorithm 2 is executed at each instance. When using (8) to find θ_i value via arc-tangent function, Algorithm 2 returns output values on the scale from $-180°$ $(-\pi)$ to $+180°$ $(+\pi)$. From this it follows that, once any of the input joint positions θ_i, $i = 1, 2, 3$, reaches $+180°$ $(+\pi)$ side, it will start from the $-180°$ $(-\pi)$ side at the next rotational instance. To ensure continuous motion trajectory, such jumps in the input joint positions' values have to be accounted by adding an extra 360° (2π) to the input joint position experiencing it, starting the instance it happened $\theta_{i,j}$, $j = 2, 3, \ldots S$, till the end of the motion trajectory $\theta_{i,S}$. As a result, the input joints trajectory $\boldsymbol{\theta}_{traj}$ that leads to a single rotation of the SPM's mobile platform around the vector $\mathbf{n}$ is generated. The infinite rotational motion of the coaxial SPM is achieved by applying the obtained input sequence $\boldsymbol{\theta}_{traj}$ repeatedly. However, each following rotation has to be adjusted by adding an extra 360° (2π) to the input sequence $\boldsymbol{\theta}_{traj}$ at the time when the ongoing rotation is finished, again, to ensure motion continuity.

Before applying the generated motion trajectories on the manipulator itself, it is necessary to verify that none of the input joint positions require any of the proximal links to surpass the neighboring ones by going through them in order to achieve corresponding orientation. An example of such link surpass is the input joints positions $\boldsymbol{\theta} = \left[200°, 150°, 100°\right]^T$, which following Algorithm 2 will be obtained as $\boldsymbol{\theta} = \left[-160°, 150°, 100°\right]^T$. In this case, the calculated input joint positions require the *proximal link 1* to move in the opposite direction comparing to the other two proximal links, resulting in its collision with the *proximal link 2* while trying to surpass it. In general, link surpass happens when one of the input joint positions is greater than the next input joint position in the positive (clockwise) direction of SPM movement, i.e. $\theta_3 - \theta_2$, $\theta_2 - \theta_1$, or $\theta_1 - \theta_3$ is not greater than 120° (the thickness of SPM links is ignored). To solve this issue an extra 360° (2π) needs to be added for the duration of the entire motion trajectory to the proximal link being the earliest in the positive (clockwise) direction.

The presented approach for the infinite rotational motion generation is summarized in Algorithm 3. It applies to the rotational motions at the desired locations that do not lead to singularities or link collisions. Details on how to check for singularities and link collisions are presented in the next section.

4. Configuration Space and Workspace Analyses

This section presents a method for numerical analysis of the coaxial SPM's configuration space and the Cartesian workspace for the case of singularity and link collision free infinite rotational motions.

4.1. Singularity Detection

As for the most of other manipulators, singularity issues need to be considered and analyzed before setting the coaxial SPM into a motion. It is necessary to keep manipulator away from singular and near-singular configurations as its controllability is weak at these points.

Singularity analysis of parallel manipulators is based on the early work of Gosselin and Angeles [55], where they described the relationship between the input and output speeds as follows:

$$\dot{\theta} = \mathbf{J}\omega, \tag{13}$$

where ω is the angular velocity vector of the mobile platform, $\dot{\theta}$ is the vector of actuated joint rates, and $\mathbf{J}$ is the Jacobian matrix that maps the angular velocity vector ω to the vector of actuated joint rates $\dot{\theta}$.

Algorithm 3: Rotational motion trajectory generation for a single rotation of a coaxial SPM

Input: $\mathbf{v}_i$, $i = 1, 2, 3$, α_1, α_2, η_i, $\boldsymbol{\sigma}$
Output: Input joints trajectory $\boldsymbol{\theta}_{traj}$

Calculate $\mathbf{n}$ using (10) given $\mathbf{v}_i$;
for $j \leftarrow 1$ **to** S **do**
  Calculate $\mathbf{v}_{i,j}$, $i = 1, 2, 3$, using (11) with σ_j and $\mathbf{n}$;
  Calculate input joint positions $\boldsymbol{\theta}_j$ for each $\mathbf{v}_{i,j}$, $i = 1, 2, 3$, using Algorithm 2;
  $\boldsymbol{\theta}_{traj}(j) \leftarrow \boldsymbol{\theta}_j$;
`/* check for 360° jumps in` $\boldsymbol{\theta}_{traj}$ `*/`
for $k \leftarrow 1$ **to** $S - 1$ **do**
  if $\theta_{1,k} - \theta_{1,k+1} > 0°$ **then**
    $\theta_{1,k+1} = \theta_{1,k+1} + 360°$;
  if $\theta_{2,k} - \theta_{2,k+1} > 0°$ **then**
    $\theta_{2,k+1} = \theta_{2,k+1} + 360°$;
  if $\theta_{3,k} - \theta_{3,k+1} > 0°$ **then**
    $\theta_{3,k+1} = \theta_{3,k+1} + 360°$;
`/* check for link surpass */`
if $\theta_{3,1} - \theta_{2,1} > 120°$ **then**
  $\theta_{2,1\ldots S} = \theta_{2,1\ldots S} + 360°$;
if $\theta_{2,1} - \theta_{1,1} > 120°$ **then**
  $\theta_{1,1\ldots S} = \theta_{1,1\ldots S} + 360°$;
if $\theta_{1,1} - \theta_{3,1} > 120°$ **then**
  $\theta_{3,1\ldots S} = \theta_{3,1\ldots S} + 360°$;
return $\boldsymbol{\theta}_{traj}$

The Jacobian matrix can be expressed as [20]

$$\mathbf{J} = -\mathbf{J}_2^{-1}\mathbf{J}_1, \tag{14}$$

which leads to the equivalent representation of (13):

$$\mathbf{J}_1\omega + \mathbf{J}_2\dot{\theta} = \mathbf{0}. \tag{15}$$

Here, $\mathbf{J}_1$ and $\mathbf{J}_2$ are both $n \times n$ Jacobian matrices ($n = 3$ for coaxial SPM), and configuration dependent, i.e., $\mathbf{J}_1 = \mathbf{J}_1(\mathbf{v}_i, \theta)$ and $\mathbf{J}_2 = \mathbf{J}_2(\mathbf{v}_i, \theta)$. For 3-RRR SPMs, these matrices are defined as [55]

$$\mathbf{J}_1 = \begin{bmatrix} (\mathbf{w}_1 \times \mathbf{v}_1)^T \\ (\mathbf{w}_2 \times \mathbf{v}_2)^T \\ (\mathbf{w}_3 \times \mathbf{v}_3)^T \end{bmatrix}, \tag{16}$$

$$\begin{aligned} \mathbf{J}_2 = diag(&\mathbf{w}_1 \times \mathbf{u}_1 \cdot \mathbf{v}_1, \\ &\mathbf{w}_2 \times \mathbf{u}_2 \cdot \mathbf{v}_2, \\ &\mathbf{w}_3 \times \mathbf{u}_3 \cdot \mathbf{v}_3). \end{aligned} \tag{17}$$

Singularities occur in the cases when either $\mathbf{J}_1$ or $\mathbf{J}_2$ or both simultaneously are singular, i.e., $\det(\mathbf{J}_1) = 0$ and/or $\det(\mathbf{J}_2) = 0$. In other words, there exist three types of singularity cases for parallel manipulators as described in more details in [55]. This methodology was used by Gosselin *et al.* in [56], where singularity loci of the *Agile Eye* SPM were analyzed. The same methodology was applied by Bai *et al.* in [57] for singularity analysis of their proposed coaxial SPM design.

All three types of singularities of parallel manipulators have different physical interpretation. The first singularity type occurs when $\det(\mathbf{J}_2) = 0$. It lies on the boundary of the Cartesian workspace, where the mobile platform loses one or more DOFs [56]. It happens when any of the SPM's legs is completely folded or unfolded, resulting in the ability of the mobile platform to resist one or more moments without exerting any torque at the input joints. The second singularity type occurs when $\det(\mathbf{J}_1) = 0$. In this configuration, the mobile platform can move despite of the actuators being locked [56]. It corresponds to configurations in which distal links either lie on the plane of the mobile platform or are orthogonal to this plane. Example of such configuration is shown in [57]'s Fig. 8. Generally, such configurations are not reachable due to the physical interference of the links. Bonev and Gosselin published the work dedicated to this type of SPM singularities [58], since they can appear inside the Cartesian workspace and require more attention. It was found out that for coaxial SPMs with $\beta = 90°$, the second singularity type can occur only when the mobile's platform tilting is $0°, 90°$, or $180°$, and only when $\alpha_1 = \alpha_2 = 90°$. The third singularity type occurs when the SPM has $\alpha_1 = \alpha_2$, and results in a situation in which actuators' motion does not lead to the motion of the mobile platform [55]. This singularity type is an architectural singularity [56]. Thus, appropriate selection of geometrical parameters of the SPM links, allows to eliminate presence of the second and the third singularity types.

In this work, conditioning index $\zeta(\mathbf{J}) \in (0, 1)$ is used to estimate proximity of a particular SPM configuration to any singularity. It is is defined as [20]:

$$\zeta(\mathbf{J}) = \frac{1}{\|\mathbf{J}\| \, \|\mathbf{J}^{-1}\|}, \tag{18}$$

where $\|\mathbf{J}\|$ is obtained as:

$$\|\mathbf{J}\| = \sqrt{tr\left(\mathbf{J}^T \frac{1}{3}\mathbf{I}\mathbf{J}\right)}, \tag{19}$$

and $\mathbf{I}$ denotes a 3×3 identity matrix.

Near-singular configurations are the ones with $\zeta(\mathbf{J})$ being close to 0, whereas non-singular configurations have $\zeta(\mathbf{J})$ equal to 1. This index is commonly used for SPM design optimization and dexterity analysis such as in [11, 59–61]. To separate near-singular configurations from non-singular configurations, a threshold value $\zeta(\mathbf{J})_{min}$ is used. This technique was previously applied by the authors to general SPM workspace computation in [49]. The same definition of the near-singularity based on a condition number of the Jacobian matrix is exploited in [62] to determine near-singular configurations of a Stewart platform.

For a sampled rotational motion of the SPM's mobile platform, $\zeta(\mathbf{J})$ is computed at each rotational instance. If any of $\zeta(\mathbf{J})$ values during the rotation is below the threshold value $\zeta(\mathbf{J})_{min}$, this rotational motion's trajectory is considered to be not singularity-free and is avoided.

4.2. Link Collision Detection

Generation of link collision free motion trajectories were considered in the author's previous works [40, 49], where two link collision detection approaches were proposed for the case of the general SPM. In [40] the SPM links are approximated by using sets of line segments with coordinates defined as a function of $\boldsymbol{\theta}$, knowing the manipulator geometry. The drawback of this method is that it gives only a rough estimate of the collision due to the link approximation that reduced overall computed configuration space. This was shown in [49] through the comparison of the SPM joint spaces, computed using the first link collision detection approach and the experimental one based on providing control inputs to a real-world SPM prototype and measuring motor supply currents. In the event of collision, the current in at least one of the actuators was sharply increasing. This approach estimates collision more accurately compared to the first one, but it requires the availability of the operational SPM prototype. Another issue with this method is that it disregards possible joint configurations that are achievable in general, but not reachable from the home configuration directly. In this work, this problem is solved by performing link collision detection on a 3D SPM prototype model in a virtual robot simulator. This approach ensures more accurate detection of link collisions at all possible configurations and is a faster process as it does not require the availability of an experimental manipulator prototype with implemented motion control.

The authors propose to model motion of the coaxial SPM prototype for kinematic analysis, link collision detection and control system development using CoppeliaSim robot simulator as detailed in [51]. In the event of the link collision, the simulator's link collision module signals that visually by coloring collided links, and can send collision flag with the IDs of the collided links to a remote client if requested to do so. CoppeliaSim's collision detection module implements the algorithm for efficient and exact interference detection amongst complex polygonal models, e.g. SPM links, based on hierarchical representation of the models using tight-fitting oriented bounding box trees. At runtime, the algorithm traverses two such trees and tests for overlaps between oriented bounding boxes [50, 63].

In this work, the CoppeliaSim collision check routine is repeated at each rotational instance of the sampled rotational motion of the coaxial SPM's 3D simulation model. If any of the manipulator's link collide during the rotational motion, this motion is treated as not safe and is avoided.

4.3. Configuration Space

The configuration space of a spherical robot-manipulator is defined as the set of all input joint positions that are feasible. Feasibility is determined based on the singularity and link collision checks. Input joint positions that do not lead to singular or near-singular configurations and do not cause link collisions are feasible.

Feasibility verification of a given configuration $\boldsymbol{\theta}$ of the coaxial SPM can be done combining the approaches for singularity and link collision detection described in the two previous subsections. The space of feasible configurations is generated numerically in this case by scanning through the 3D grid of all possible combinations of input joint positions and performing feasibility test at each node. Unfeasible configurations are not included in the configuration space.

The coordinates of the 3D grid's nodes belong to sets

$$\boldsymbol{\phi}_i = \{\theta_{i,1},\ \theta_{i,2},\ \ldots\ \theta_{i,M_i}\}, \quad i = 1, 2, 3, \tag{20}$$

where M_i indicates the size of the set to which a particular input joint position θ_i belongs to. A uniform sampling interval of the joint configurations is employed for the simplicity of the numerical analysis, i.e., $\delta_\phi \triangleq \theta_{i,j+1} - \theta_{i,j}$, $j = 1, 2, ... M_i - 1$ is constant, and $M_1 = M_2 = M_3$.

As was discussed in Section 3, some joint configurations may cause the link surpass. To reduce the computational burden, nodes representing such configurations can be excluded right away without performing feasibility tests on them, since no physical manipulator is capable of performing link surpass motions in the real world. The remaining nodes are subjects of the singularity and link collision checks.

After performing feasibility verification procedure on all nodes of the 3D grid, a set $\mathcal{V}$, that represents the union of all feasible joint configurations of the coaxial SPM, is created. This procedure is presented in Algorithm 4. Computation of the set $\mathcal{V}$ allows evaluation of control limits of a manipulator and dependencies between each actuator, i.e., safety margins for actuators' operation. This set can also be used to generate optimal motion trajectories for control purposes, e.g. shortest path in joint space.

4.4. Cartesian Workspace

Cartesian workspace analysis allows to find the physical limits of the SPM's mobile platform's motion. It represents a collection of the locations that are reachable by the coaxial SPM prototype and where its infinite rotational motion is possible.

In order to numerically evaluate the coaxial SPM's workspace, a grid of points $\mathcal{W}_{temp}$ is generated. In this work, an icosahedral grid [64] normalized to a unit sphere is selected. This grid provides almost-equally distributed test nodes, and contains the Cartesian coordinates of each one of them. The interval between test nodes is determined based on the applied g-level (grid division level). The number of test nodes is $N = 2 \times 10^{2l} + 2$, where $l = \{0, 1, 2, 3, 4, ...\}$ is the g-level. The average interval is equal to $\frac{1}{2^l}\sqrt{\frac{2\pi}{5}}$. If lower precision for the Cartesian workspace is acceptable, it is worth increasing the interval between nodes by selecting lower g-level value to reduce processing time.

At each test node, the unit vectors $\mathbf{v}_i$, $i = 1, 2, 3$, are reconstructed by selecting vector $\mathbf{v}_1$ that is defined by the cross product of the test node position (i.e. its Cartesian coordinates as normal vector $\mathbf{n}$)

Algorithm 4: Numerical computation of the configuration space of a coaxial SPM

Input: α_1, α_2, β, $\boldsymbol{x}_0$, η_i, ϕ_i, $i = 1, 2, 3$
Output: Set $\mathcal{V}$

```
V ← ∅;
for a1 ← 1 to M1 do
    for a2 ← 1 to M2 do
        for a3 ← 1 to M3 do
            singularity ← false;
            collision ← false;
            /* link surpass check                    */
            if θ3(a3) − θ2(a2) > 120° or
             θ2(a2) − θ1(a1) > 120° or
             θ1(a1) − θ3(a3) > 120° then
                collision ← true
                break
            θ ← [θ1(a1)  θ2(a2)  θ3(a3)]^T;
            /* forward kinematics                    */
            Calculate w_i and v_i, i = 1, 2, 3,
             given θ using Algorithm 1;
            /* singularity detection                 */
            Calculate J given u_i, w_i and v_i,
             i = 1, 2, 3, following (14)-(17);
            Calculate ζ(J) given J, following
             (18) and (19);
            if ζ(J) < ζ(J)_min then
                singularity ← true
                break
            /* link collision detection              */
            Send θ to the coaxial SPM
             motion simulator;
            if collision handle == 1 then
                collision ← true
                break
            /* update the space                      */
            if singularity == false and
             collision == false then
                V ← V ∪ {θ}
return V
```

and the vector pointing in the positive z direction:

$$\mathbf{v}_1 = \frac{\mathbf{n} \times \begin{bmatrix}0, 0, 1\end{bmatrix}^T}{\|\mathbf{n} \times \begin{bmatrix}0, 0, 1\end{bmatrix}^T\|}. \tag{21}$$

Remaining vectors $\mathbf{v}_2$ and $\mathbf{v}_3$ are found using the Rodrigues' rotation formula as follows:

$$\begin{aligned}\mathbf{v}_2 = &\mathbf{v}_1 \cos 120^\circ + (\mathbf{n} \times \mathbf{v}_1) \sin 120^\circ + \\ &+ \mathbf{n}(\mathbf{n} \cdot \mathbf{v}_1)(1 - \cos 120^\circ),\end{aligned} \tag{22}$$

$$\mathbf{v}_3 = \mathbf{v}_1 \cos 240^\circ + (\mathbf{n} \times \mathbf{v}_1) \sin 240^\circ + \\ + \mathbf{n}(\mathbf{n} \cdot \mathbf{v}_1)(1 - \cos 240^\circ). \quad (23)$$

Subsequently, an input sequence $\boldsymbol{\theta}_{traj}$ leading to a single 360° rotational rotation is calculated from the unit vectors $\mathbf{v}_{i,rot}$, $i = 1, 2, 3$ using (11) and Algorithm 2 for obtaining unique inverse kinematics solutions. At each test nodes, all rotational instances of the sampled rotational motion are checked for singularity and link collision using approaches outlined in the previous subsection (Sections 4.1 and 4.2). After evaluating each test node belonging to set $\mathcal{W}_{temp}$, and selecting singularity and collision free test nodes, a set $\mathcal{W}$, representing the union of all nodes corresponding to the coaxial SPM's Cartesian workspace, is obtained. Algorithm 5 details the procedure for determining set $\mathcal{W}$.

Algorithm 5: Numerical computation of the Cartesian workspace of a coaxial SPM

Input: l, $\boldsymbol{\sigma}$, α_1, α_2, β, $\boldsymbol{x}_0$, η_i, $i = 1, 2, 3$
Output: Set $\mathcal{W}$

$\mathcal{W} \leftarrow \emptyset$;
$\mathcal{W}_{temp} \leftarrow$ icosahedral grid generated using [64];
for $j \leftarrow 1$ **to** N **do**
  $singularity \leftarrow false$;
  $collision \leftarrow false$;
  Set test node coordinates as $\mathbf{n} = \mathcal{W}_{temp}(j)$;
  Reconstruct $\mathbf{v}_{i,j}$, $i = 1, 2, 3$, following (21)-(23);
  Generate rotational motion trajectory $\boldsymbol{\theta}_{traj}$ for a single rotation given $\mathbf{v}_{i,j}$, $i = 1, 2, 3$, using Algorithm 3;
  `/* singularity detection */`
  for $k \leftarrow 1$ **to** S **do**
    Calculate $\mathbf{w}_{i,j,k}$ and $\mathbf{v}_{i,j,k}$, $i = 1, 2, 3$, given $\boldsymbol{\theta}_{traj}(k)$ using Algorithm 1;
    Calculate $\mathbf{J}$ given $\mathbf{u}_{i,j,k}$, $\mathbf{w}_{i,j,k}$ and $\mathbf{v}_{i,j,k}$, $i = 1, 2, 3$, following (14)-(17);
    Calculate $\zeta(\mathbf{J})$ given $\mathbf{J}$, following (18) and (19);
    if $\zeta(\boldsymbol{J}) < \zeta(\boldsymbol{J})_{min}$ **then**
      $singularity \leftarrow true$
      break
  if $singularity == true$ **then**
    break
  `/* link collision detection */`
  Send $\boldsymbol{\theta_{traj}}$ to robot simulator;
  if *collision handle* $== 1$ **then**
    $collision \leftarrow true$
    break
  `/* update the workspace */`
  if $singularity == false$ **and** $collision == false$ **then**
    $\mathcal{W} \leftarrow \mathcal{W} \cup \mathbf{n}$
return $\mathcal{W}$

5. Simulation Model and Experimental Prototype

Numerical verification of the presented framework is done via simulations and experiments using a coaxial SPM prototype with the following geometrical parameters: $\alpha_1 = 45^\circ$, $\alpha_2 = 90^\circ$, $\beta = 90^\circ$, and $\gamma = 0^\circ$. These parameters were selected such that they approximately match one of the Pareto-optimal SPM design solutions (Design ID I: $\alpha_1 = 47.2^\circ$, $\alpha_2 = 91.7^\circ$, $\beta = 88.4^\circ$, $\gamma = 0^\circ$) presented in [32], where a multiobjective design optimization problem was formulated to determine the coaxial SPM configuration with minimum mass and increased dexterity. The selected SPM parameters for the experimental manipulator prototype will also allow to make future comparison (dynamic, stiffness, etc.) with the SPM design prototype proposed in [32]. Selection of the geometrical parameters with $\alpha_1 \neq \alpha_2$ helps to avoid the second and the third singularity types as mentioned earlier in Section 4.1.

A CAD model of the manipulator with these parameters was created in SolidWorks 3D modeling software and is shown in Fig. 3a. For the link collision detection purposes, this model was simplified by removing non-crucial design details such as fixtures, interior holes, gear teeth, and afterwards imported to CoppeliaSim (V-REP) robot simulator (Fig. 3b) for link collision detection as detailed in Section 4.2 and [51]. MATLAB was used for motion control of the simulation model, collision data recording, and singularity detection calculations.

In order to create the simulation model of the coaxial SPM, the CAD model was saved in STL format in SolidWorks and a single combined manipulator assembly was imported to CoppeliaSim, where it was divided into several parts corresponding to the manipulator's links. The resulting model

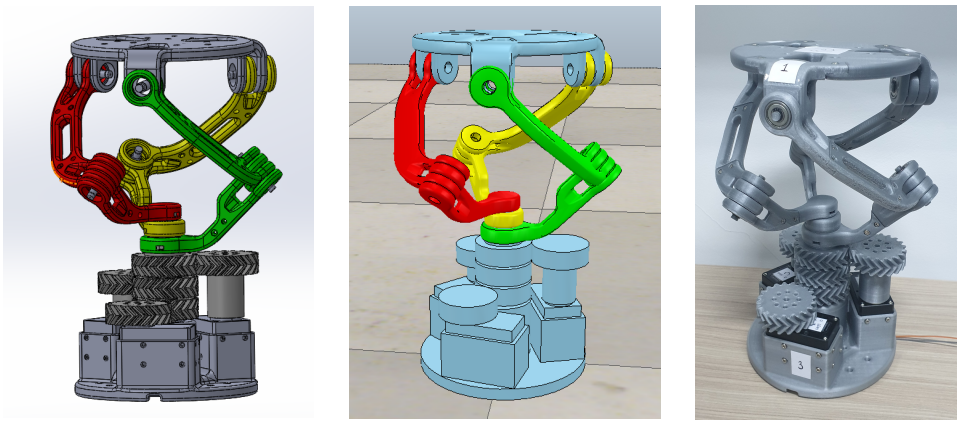

(a) (b) (c)

Figure 3: Coaxial SPM: (a) CAD model, (b) simulation model, (c) 3D-printed experimental prototype.

of the coaxial SPM consists of 8 shapes: the base, 3 distal links, 3 proximal links, and the mobile platform. Actuators and gears were combined with the base and do not play a role in the manipulator's actuation in this model. Actuation is done through proximal links. In the last steps of the simulation model preparation, it was assembled resembling the closed-loop kinematic architecture of the manipulator. There are 2 closed loops in the model, i.e. *base - proximal link 3 - distal link 3 - mobile platform - distal link 1 - proximal link 1 - base* and *base - proximal link 3 - distal link 3 - mobile platform - distal link 2 - proximal link 2 - base*. Additional details about CoppeliaSim settings and its linkage to MATLAB can be found in [51].

3D-printing rapid prototyping technology, i.e. PLA plastic filament and Ultimaker Extended 2+ 3D-printer, was used for manufacturing mechanical elements of the coaxial SPM's experimental prototype shown in (Fig. 3c). Actuation of the input joints is performed by three ROBOTIS Dynamixel XM540-W150 servomotors that are equidistantly located on the manipulator's base. The servomotors are controlled via MATLAB using Dynamixel SDK (Protocol 2.0) API.

Unlike the author's previous SPM prototype utilized in [37], the new coaxial SPM prototype uses double helical gears (herringbone gears) with the input joints instead of simple spur gears as before for smoother motion and reduced backlash [65].

6. Results and Discussion

6.1. Configuration Space Computation

The configuration space of the feasible input joint positions was obtained by confirming that a given input vector $\boldsymbol{\theta}$ does not bring the coaxial SPM to singularity/near-singularity or does not result in link collisions as outlined in Algorithm 4. The 3D grid of test nodes was limited by input values of 0° and 360° with a step $\delta_\phi = 5°$, that resulted in a total of 373,248 test nodes. Figure 4 presents intermediate and final sets of the configuration space at each stage of its computation. The initial set was obtained, as shown in Fig. 4a, after eliminating SPM configurations that result in link surpass. It was found out that in one of the directions, the set under study has an identical cross-sectional profile shape, shown in Fig. 4a as a shaded circle in the 3D plot and separately underneath the figure. This direction corresponds to the line connecting the test nodes $\boldsymbol{\theta} = \left[0°,\ 0°,\ 0°\right]^T$ and $\boldsymbol{\theta} = \left[360°,\ 360°,\ 360°\right]^T$, which is one of the 3D diagonals of the initial cubical 3D grid. This line also corresponds to the trajectory of the infinite rotational motion of the mobile platform around z-axis, as will be shown in Section 6.3.3. Afterwards, remaining test nodes were tested for singularity with the threshold conditioning index $\zeta(\mathbf{J})_{min} = 0.2$. Singularity detection routine resulted in appearance of several disconnected smaller subsets as shown in Fig. 4b (cross-sectional view). These subsets belong to the different assembly modes of the coaxial SPM. Subsequently, the singularity-free configurations were tested for link collisions via simula-

tions in CoppeliaSim. The final set of the feasible input joint positions $\mathcal{V}$, i.e configuration space of the coaxial SPM's prototype, was computed and is presented in Fig. 4c. The sets in Figs. 4b and 4c demonstrate the same invariability of the cross-sections on that particular diagonal.

Analysis of the computed set $\mathcal{V}$ of the feasible configurations shows that it stretches from the node $\boldsymbol{\theta} = \left[0^\circ,\ 0^\circ,\ 0^\circ\right]^T$ to the node $\boldsymbol{\theta} = \left[360^\circ,\ 360^\circ,\ 360^\circ\right]^T$ with the variability of each input joint position not greater than 100° from the straight line connecting those two nodes. From this it follows that specifically for the coaxial SPM's prototype under study its actuators' inputs can not vary from each other by more than ±100°, otherwise some of the links will collide. It needs to be mentioned that the obtained set $\mathcal{V}$ expends infinitely in the positive and negative directions following the $\left[0^\circ,\ 0^\circ,\ 0^\circ\right]^T$ - $\left[360^\circ,\ 360^\circ,\ 360^\circ\right]^T$ line and having the same cross-sectional view profile. This result confirms the fact that the coaxial SPM is capable of the infinite rotational motion, and trajectories leading to it are not bounded on the diagonal direction, meaning that such trajectories can go beyond the tested set bounded by $\theta_i \subseteq [0^\circ, 360^\circ], i = 1, 2, 3$ (example of this is shown in Case 3 of the accompanying video).

6.2. Cartesian Workspace Computation

The Cartesian workspace was estimated by verifying whether any rotational instance of the infinite rotational motion of the coaxial SPM in this location brings SPM to a singularity or near-singularity or causes link collisions as outlined in Algorithm 5.

An icosahedral grid of test nodes $\mathcal{W}_{temp}$ was generated with g-level $l = 5$ or $factor = 32$, meaning that each triangle of the icosahedron is subdivided into 32×32 subtriangles, resulting in a total of 10,242 test nodes around the whole unit sphere. At each node, rotation of the unit vectors $\mathbf{v}_i$, $i = 1, 2, 3$, was sampled into 360 instances ($\delta_\sigma = 1^\circ$). At each instance, unique input joint positions were calculated using Algorithm 2. This way the input sequences $\boldsymbol{\theta}_{traj}$ providing a single 360° rotation of the SPM mobile platform at each test node were generated. It was found out that some input sequences contained values with imaginary parts, so the test nodes resulting in it were excluded from the rest of the analysis as they correspond to an unattainable region. Furthermore, test nodes on the negative side of the unit sphere were also excluded from the analysis as it is expected that the manipulator cannot operate in that region safely (physical limitation).

The remaining test nodes were checked for singularity and benchmarked by the conditioning index $\zeta(\mathbf{J})_{min} = 0.2$. In the case of the rotational motion, the conditioning index $\zeta(\mathbf{J})$ is not a constant value. It changes with each rotational instance (please refer to Section 6.3 and Fig. 10b and Fig. 10a). Figures 5a and 5b illustrate test nodes checked for singularity from different view points. The test nodes here represent the vector direction for $\mathbf{n}$. In these figures, the red squares indicate the test nodes at which at least one of the rotational instances has the conditioning index $\zeta(\mathbf{J})$ below $\zeta(\mathbf{J})_{min} = 0.2$. Figure 5c and 5d present the computed Cartesian workspaces (set $\mathcal{W}$) of the coaxial SPM's normalized to a unit sphere. In these figures, the red squares indicate the test nodes with link collisions during the rotation of the mobile platform. The obtained data reveals that for the given coaxial SPM's prototype the lowest tilt of the mobile platform with full rotation corresponds to 39°. In order to obtain the Cartesian workspace corresponding to the physical dimensions of the SPM's model, the obtained workspace has to be scaled by the distance from the *center of rotation* to a desired point on the SPM's mobile platform.

6.3. Infinite Rotational Motion Generation

Three case studies of the infinite rotational motion generation of the coaxial SPM prototype at a central, middle and edge regions of its Cartesian workspace are presented to demonstrate the proposed computational framework.

6.3.1. Case Study 1: Infinite Rotational Motion in the Edge Region of the SPM Cartesian Workspace

A Cartesian workspace test node $\mathbf{n} = \left[-0.274,\ -0.555,\ 0.786\right]^T$ is used in this example. It corresponds to 38.22° tilt of the SPM mobile platform as shown in Fig. 6a, where vector $\mathbf{z}$ represents z-axis of the coordinate system and vector $\mathbf{n}$ represents normal vector of the mobile platform shown from the center of rotation. The unit vectors $\mathbf{v}_i$, $i = 1, 2, 3$, corresponding to one of the possible orientations of the mobile platform at this test node

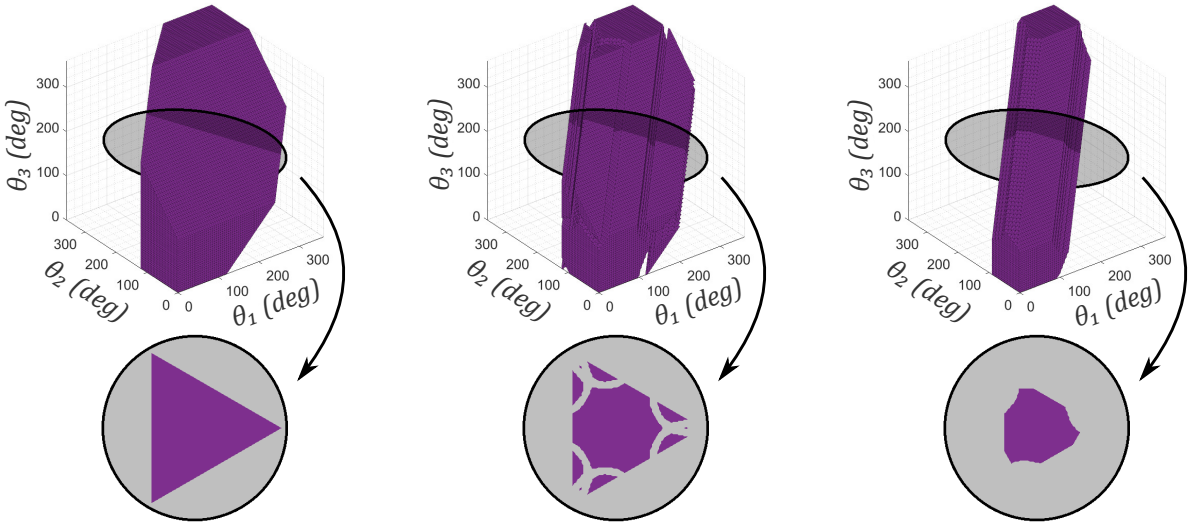

Figure 4: Sets with cross-sectional views obtained at different stages of the computation process of the Coaxial SPM's feasible configuration space: (a) set of test nodes with no link surpass, (b) set of singularity free test nodes, (c) set of link collision free test nodes.

are computed following (21)-(23):

$$\begin{aligned} \mathbf{v}_1 &= \big[-0.8967,\, 0.4427,\, 0.0000\big]^T, \\ \mathbf{v}_2 &= \big[0.1471,\, -0.8314,\, -0.5358\big]^T, \\ \mathbf{v}_3 &= \big[0.7495,\, 0.3887,\, 0.5358\big]^T. \end{aligned} \tag{24}$$

Once these unit vectors are obtained, the procedure is continued with Algorithm 3. Rotational instances of the unit vectors (24), $\mathbf{v}_{i,rot}$, $i = 1, 2, 3$, are calculated by applying (11) for a single 360° rotation cycle with $\delta_\sigma = 1°$. The input joint positions vector $\boldsymbol{\theta}$ is then calculated by applying Algorithm 2 at each rotational instance. The generated input joint trajectory $\boldsymbol{\theta}_{traj}$ is shown in Fig. 7a in the form of a helix-shaped path inside the SPM feasible configurations space, obtained in Section 6.1. The generated trajectory almost reaches the side edges of the feasible configuration space, indicating that the coaxial SPM is operating near the edge of its workspace. For consistency of all presented case studies, all generated trajectories are shown within the SPM feasible configuration space bounded by input joint positions 0° and 360°.

Figure 8a illustrates the sequence evolution of the generated joint positions $\boldsymbol{\theta}_{traj}$ for the three input joints of the SPM prototype, whereas Fig. 9a presents the input joint rates of position change, calculated as $\theta_{i,j+1}$ - $\theta_{i,j}$. Input joint rates of change are periodic and identical to each other with 120° phase shifts between them. It means that only one input joint position can be generated; the remaining input joint positions are obtained by adding 120° and 240° phase shifts. A similar periodic behavior during the SPM rotational motion is observed in the sample evolution of the conditioning index $\zeta(\mathbf{J})$ shown in Fig. 10a. It implies that during the infinite rotational motion of the coaxial SPM the conditioning index is not constant and can go beyond the threshold value, which indicates that the motion can be unfeasible.

The generated input joint trajectories were first tested on the coaxial SPM model in CoppeliaSim robot simulator resulting in the dynamic visualization of the expected infinite rotation of the manipulator as presented in Fig. A.11 as SPM model subsequent positions at six input joint trajectory instances. Time evolution of unit vectors $\mathbf{v}_i$, $i = 1, 2, 3$, characterizing the instantaneous orientation of the coaxial SPM model during the rotational motion simulation, were compared with the numerically computed reference vectors $\mathbf{v}_{i,rot}$, $i = 1, 2, 3$, similarly to the procedure, presented in [51]. The ideal matching of both the simulated and the precomputed desired rotational motion trajectories of the coaxial SPM model orientation vectors verifies the correctness and pointing accuracy of the pro-

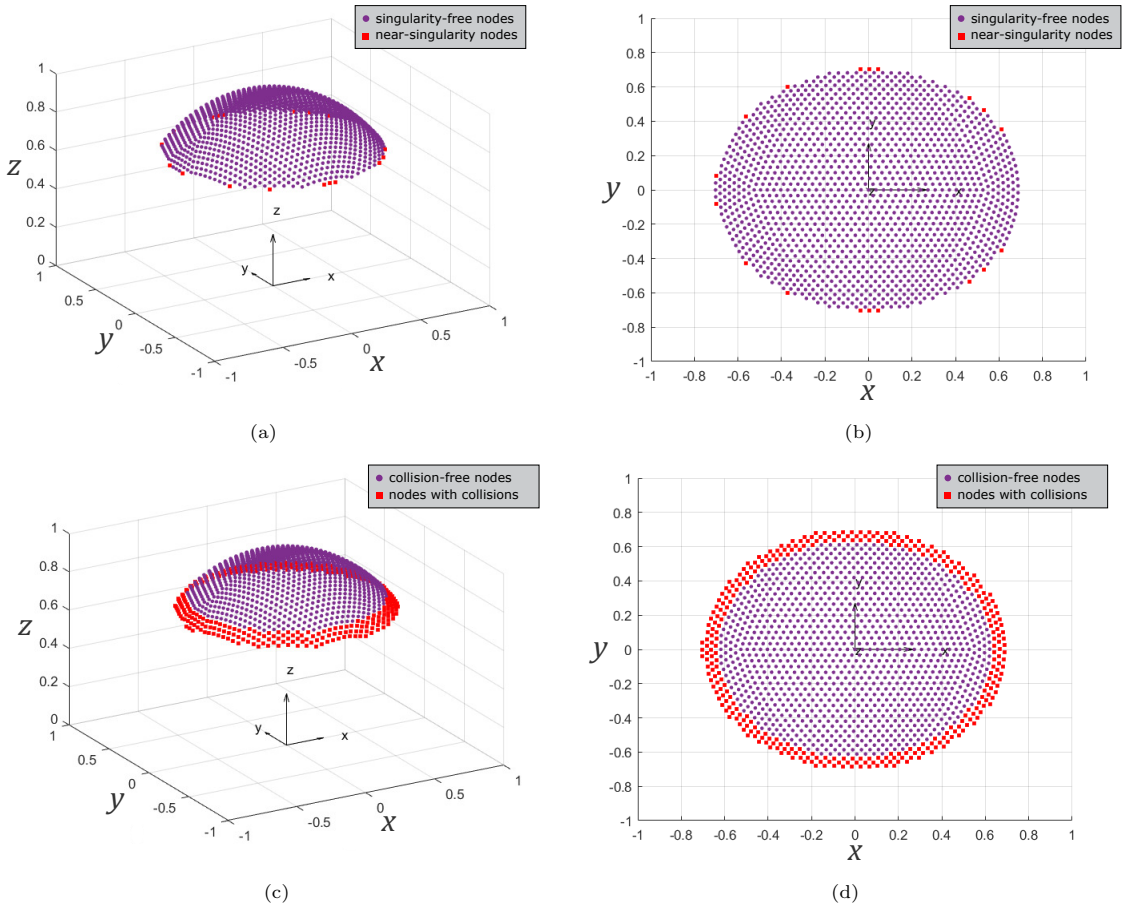

Figure 5: Sets with top views obtained at different stages of the computation process of the coaxial SPM's Cartesian workspace: (a) set of singularity-free and near-singular test nodes, (b) top view of the previous set, (c) set of link collision-free test nodes and nodes with link collisions, (d) top view of the previous set.

posed numerical framework for generating input joint trajectories, that are used as actuated joint references for realizing infinite rotational motion of the coaxial SPM's top mobile platform around its normal vector in a desired orientation.

The input trajectories were also applied on the experimental prototype of the coaxial SPM as shown in Fig. A.12 in the same format. The complete rotation coaxial SPM prototype is presented in the accompanying video demonstration. The visual demonstration on the experimental prototype confirmed the overall correctness of the proposed framework assuming an open loop control approach. Design of a closed loop orientation control system for eliminating the effects of manipulator's dynamics, potential frictions in transmission gears and joints and mechanical inaccuracies in the physical SPM prototype on its pointing accuracy is beyond the scope of this work and is the subject of the authors' future research.

6.3.2. Case Study 2: Infinite Rotational Motion in the Middle Region of the SPM Cartesian Workspace

Consider the test node $\mathbf{n} = [0.165,\ -0.326,\ 0.931]^T$ on the Cartesian workspace of the coaxial SPM prototype, corresponding to 21.43° tilt of the mobile platform as shown in Fig. 6b. Similarly to Case Study 1, the generated trajectory, input joint positions and rates of change, conditioning index $\zeta(\mathbf{J})$ for this case study are computed and presented in Figs. 7b, 8b, 9b, 10b, respectively. The snapshots of the resulting rotation of the coaxial SPM simulator model and experimental prototype are presented in Fig. A.13 and Fig. A.14, respectively.

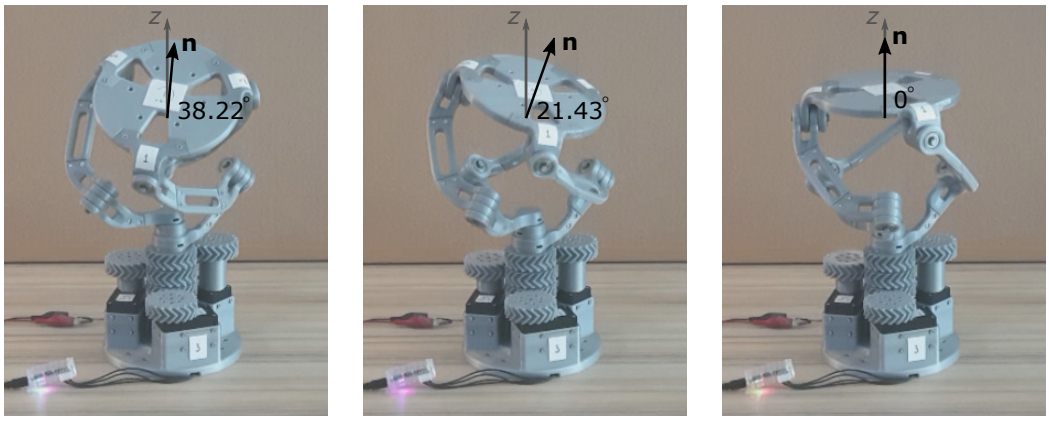

(a) (b) (c)

Figure 6: Case studies of the infinite rotational motion generation of the coaxial SPM prototype: (a) case study 1 with $\mathbf{n} = [-0.274, -0.555, 0.7861]^T$, (b) case study 2 with $\mathbf{n} = [0.165, -0.326, 0.931]^T$, (c) case study 3 with $\mathbf{n} = [0, 0, 1]^T$.

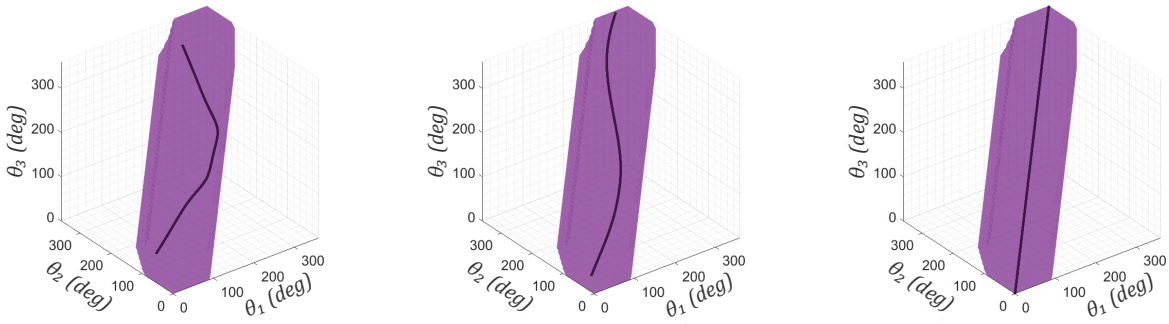

(a) (b) (c)

Figure 7: Generated rotational motion joint trajectories of the coaxial SPM prototype: (a) case study 1 with $\mathbf{n} = [-0.274, -0.555, 0.786]^T$, (b) case study 2 with $\mathbf{n} = [0.165, -0.326, 0.931]^T$, (c) case study 3 with $\mathbf{n} = [0, 0, 1]^T$.

6.3.3. Case Study 3: Infinite Rotational Motion in the Central Region of the SPM Cartesian Workspace

Consider the test node $\mathbf{n} = \begin{bmatrix} 0, & 0, & 1 \end{bmatrix}^T$, corresponding to 0° tilt of the mobile platform as shown in Fig. 6c. Similarly to Case Study 1, the generated trajectory, input joint positions and rates of change, conditioning index $\zeta(\mathbf{J})$ for this case study are computed and presented in Figs. 7c, 8c, 9c, 10c, respectively. In this case, input joint rates of changes and conditioning index $\zeta(\mathbf{J})$ are constant values, and the input trajectory is a straight line connecting nodes $\begin{bmatrix} 0, & 0, & 0 \end{bmatrix}^T$ and $\begin{bmatrix} 360, & 360, & 360 \end{bmatrix}^T$. The snapshots of the resulting rotation of the coaxial SPM simulator model and experimental prototype are presented in Fig. A.15 and Fig. A.16, respectively.

7. Conclusion

This paper presented in detail a novel framework for infinite rotational motion generation and kinematic analysis of a 3-RRR SPM with coaxial input shafts. At first, a revised approach for obtaining unique kinematics solutions was presented, based on which a novel approach for generating infinite rotational motion of the coaxial SPM top mobile platform was formalized and verified via simulations and experimental tests of a coaxial SPM model and its physical prototype, respectively, thus demonstrating its practical applicability to designing SPM based mechanisms with infinite rotational motion capabilities.

The obtained numerical results revealed periodic nature and similarities between the input joint rates of change of the employed coaxial SPM model.

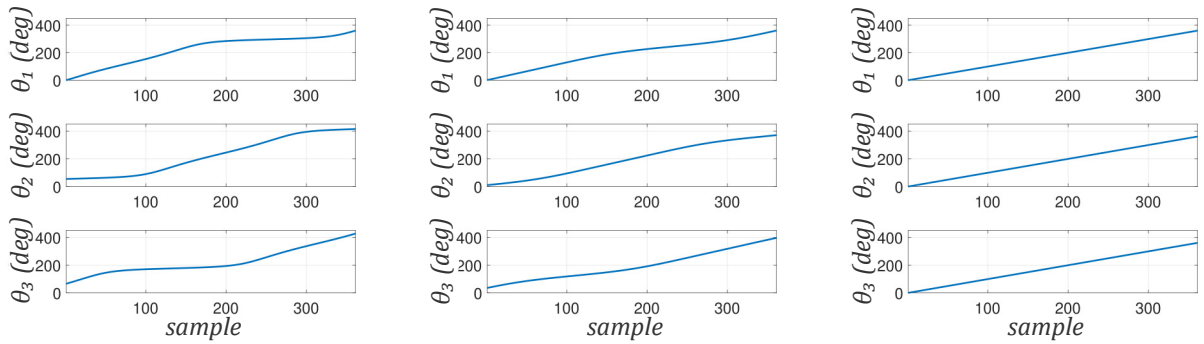

(a) (b) (c)

Figure 8: Evolution of the input joint positions of the coaxial SPM prototype: (a) case study 1 with $\mathbf{n} = [-0.274, -0.555, 0.786]^T$, (b) case study 2 with $\mathbf{n} = [0.165, -0.326, 0.931]^T$, (c) case study 3 with $\mathbf{n} = [0, 0, 1]^T$.

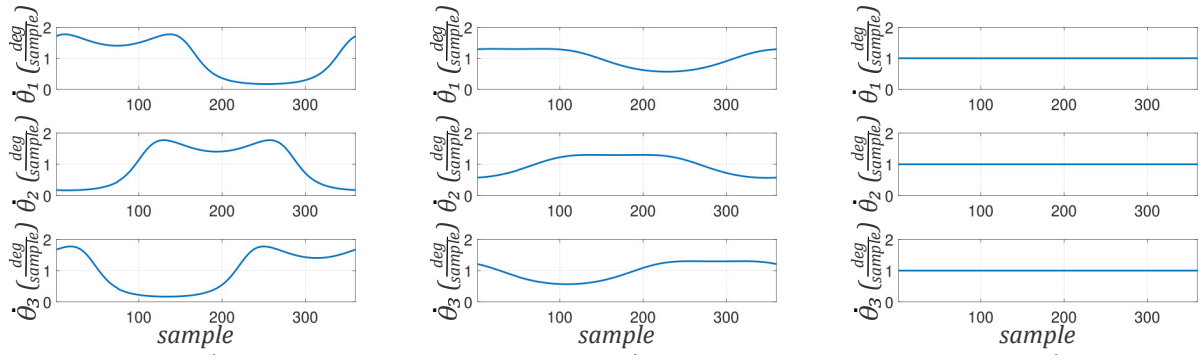

(a) (b) (c)

Figure 9: Evolution of the input joint rates of change of the coaxial SPM prototype: (a) case study 1 with $\mathbf{n} = [-0.274, -0.555, 0.786]^T$, (b) case study 2 with $\mathbf{n} = [0.165, -0.326, 0.931]^T$, (c) case study 3 with $\mathbf{n} = [0, 0, 1]^T$.

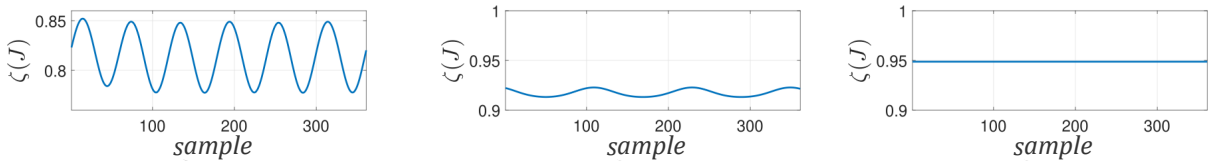

(a) (b) (c)

Figure 10: Evolution of the conditioning index $\zeta(\mathbf{J})$ of the coaxial SPM prototype: (a) case study 1 with $\mathbf{n} = [-0.274, -0.555, 0.786]^T$, (b) case study 2 with $\mathbf{n} = [0.165, -0.326, 0.931]^T$, (c) case study 3 with $\mathbf{n} = [0, 0, 1]^T$.

Spatial analysis of the coaxial SPM model taking into account infinite rotational motion capability of the manipulator was performed resulting in the numerically computed joint and Cartesian workspaces of the manipulator excluding singularity, near-singularity and link collision robot configurations. For the particular SPM prototype under study, it was found that its maximum Cartesian workspace is limited by 39° tilt.

In this work, only the visual verification of the proposed framework on the experimental coaxial SPM's prototype is presented assuming an open loop control approach without correcting manipulator's dynamics, potential friction in transmission gears and joints and mechanical inaccuracies, that would affect the pointing accuracy of real-life system. As a future work the presented coaxial SPM infinite rotational motion generation and kinematic analysis framework will be further utilized for designing the manipulator's real-time orientation con-

trol system with integrating 6-DOF orientation sensors into the SPM mechanical prototype for a feedback control loop implementation similarly to author's previous work [49]. As part of this work an orientation accuracy analysis of the experimental coaxial SPM prototype will be conducted.

References

[1] T. Huang, Z. Li, M. Li, D. G. Chetwynd, C. M. Gosselin, Conceptual design and dimensional synthesis of a novel 2-DOF translational parallel robot for pick-and-place operations, Journal of Mechanical Design 126 (3) (2003) 449–455.

[2] J. Wu, J. Wang, L. Wang, T. Li, Dynamics and control of a planar 3-DOF parallel manipulator with actuation redundancy, Mechanism and Machine Theory 44 (4) (2009) 835–849.

[3] J. Wu, J. Wang, L. Wang, Z. You, Performance comparison of three planar 3-DOF parallel manipulators with 4-RRR, 3-RRR and 2-RRR structures, Mechatronics 20 (4) (2010) 510–517.

[4] W. Dong, Z. Du, Y. Xiao, X. Chen, Development of a parallel kinematic motion simulator platform, Mechatronics 23 (1) (2013) 154–161.

[5] J. Wu, Y. Gao, B. Zhang, L. Wang, Workspace and dynamic performance evaluation of the parallel manipulators in a spray-painting equipment, Robotics and Computer-Integrated Manufacturing 44 (2017) 199–207.

[6] N. M. Bajaj, A. J. Spiers, A. M. Dollar, State of the art in artificial wrists: A review of prosthetic and robotic wrist design, IEEE Transactions on Robotics 35 (1) (2019) 261–277.

[7] S. Bai, X. Li, J. Angeles, A review of spherical motion generation using either spherical parallel manipulators or spherical motors, Mechanism and Machine Theory 140 (2019) 377–388.

[8] G. Wu, S. Bai, Design and kinematic analysis of a 3-RRR spherical parallel manipulator reconfigured with four–bar linkages, Robotics and Computer-Integrated Manufacturing 56 (2019) 55–65.

[9] C. M. Gosselin, J.-F. Hamel, The Agile Eye: a high-performance three-degree-of-freedom camera-orienting device, in: Proceedings of the 1994 IEEE International Conference on Robotics and Automation (ICRA), 1994, pp. 781–786.

[10] H. Saafi, M. A. Laribi, S. Zeghloul, Optimal torque distribution for a redundant 3-RRR spherical parallel manipulator used as a haptic medical device, Robotics and Autonomous Systems 89 (2017) 40–50.

[11] A. Chaker, A. Mlika, M. A. Laribi, L. Romdhane, S. Zeghloul, Synthesis of spherical parallel manipulator for dexterous medical task, Frontiers of Mechanical Engineering 7 (2) (2012) 150–162.

[12] Y. Du, R. Li, D. Li, S. Bai, An ankle rehabilitation robot based on 3-RRS spherical parallel mechanism, Advances in Mechanical Engineering 9 (8) (2017) 1–8.

[13] M. Malosio, S. P. Negri, N. Pedrocchi, F. Vicentini, M. Caimmi, L. M. Tosatti, A spherical parallel three degrees-of-freedom robot for ankle-foot neuro-rehabilitation, in: 2012 Annual International Conference of the IEEE Engineering in Medicine and Biology Society, 2012, pp. 3356–3359.

[14] Y. Fang, L.-W. Tsai, Structure synthesis of a class of 3-DOF rotational parallel manipulators, IEEE Transactions on Robotics and Automation 20 (1) (2004) 117–121.

[15] X. Kong, C. M. Gosselin, Type synthesis of 3-DOF spherical parallel manipulators based on screw theory, Journal of Mechanical Design 126 (1) (2004) 101–108.

[16] X. Kong, C. M. Gosselin, Type synthesis of three-degree-of-freedom spherical parallel manipulators, The International Journal of Robotics Research 23 (3) (2004) 237–245.

[17] M. Karouia, J. M. Hervé, Non-overconstrained 3-DOF spherical parallel manipulators of type: 3-RCC, 3-CCR, 3-CRC, Robotica 24 (01) (2005) 85–94.

[18] Y. Qi, T. Sun, Y. Song, Y. Jin, Topology synthesis of three-legged spherical parallel manipulators employing Lie group theory, Proceedings of the Institution of Mechanical Engineers, Part C: Journal of Mechanical Engineering Science 229 (10) (2014) 1873–1886.

[19] C. M. Gosselin, J. Angeles, The optimum kinematic design of a spherical three-degree-of-freedom parallel manipulator, Journal of Mechanisms, Transmissions, and Automation in Design 111 (2) (1989) 202–207.

[20] C. M. Gosselin, E. Lavoie, On the kinematic design of spherical three-degree-of-freedom parallel manipulators, The International Journal of Robotics Research 12 (4) (1993) 394–402.

[21] C. M. Gosselin, J. Sefrioui, M. J. Richard, On the direct kinematics of spherical three-degree-of-freedom parallel manipulators of general architecture, Journal of Mechanical Design 116 (2) (1994) 594–598.

[22] C. M. Gosselin, E. St-Pierre, M. Gagne, On the development of the Agile Eye, IEEE Robotics & Automation Magazine 3 (4) (1996) 29–37.

[23] L. Birglen, C. M. Gosselin, N. Pouliot, B. Monsarrat, T. Laliberte, SHaDe, a new 3-DOF haptic device, IEEE Transactions on Robotics and Automation 18 (2) (2002) 166–175.

[24] G. Wu, P. Zou, Comparison of 3-DOF asymmetrical spherical parallel manipulators with respect to motion/force transmission and stiffness, Mechanism and Machine Theory 105 (2016) 369–387.

[25] H. Asada, J. Granito, Kinematic and static characterization of wrist joints and their optimal design, in: Proceedings of the 1985 IEEE International Conference on Robotics and Automation (ICRA), Vol. 2, 1985, pp. 244–250.

[26] C. M. Gosselin, J. Sefrioui, M. Richard, On the direct kinematics of spherical three-degree-of-freedom parallel manipulators with a coplanar platform, Journal of Mechanical Design 116 (2) (1994) 587–593.

[27] E. Cavallo, R. C. Michelini, V. F. Filaretov, Conceptual design of an AUV equipped with a three degrees of freedom vectored thruster, Journal of Intelligent and Robotic Systems 39 (2004) 365–391.

[28] B. Sudki, M. Lauria, F. Noca, Robotic penguin-like propulsor with novel spherical joint, in: Proceedings of the Third International Symposium on Marine Propulsors, 2013.

[29] J. Lee, J. Noh, S. Lee, W. Yang, A novel 4-DoF robotic link mechanism with E-CoSMo: kinematics based torque analysis, in: 2019 IEEE/RSJ International Conference on Intelligent Robots and Systems (IROS),

2019, pp. 3577–3582.
[30] S. Bai, M. R. Hansen, Evaluation of workspace of a spherical robotic wrist, in: 2007 IEEE/ASME International Conference on Advanced Intelligent Mechatronics (AIM), 2007, pp. 1–6.
[31] S. Bai, Optimum design of spherical parallel manipulators for a prescribed workspace, Mechanism and Machine Theory 45 (2) (2010) 200–211.
[32] G. Wu, S. Caro, S. Bai, J. Kepler, Dynamic modeling and design optimization of a 3-DOF spherical parallel manipulator, Robotics and Autonomous Systems 62 (10) (2014) 1377–1386.
[33] J. Enferadi, A. Shahi, On the position analysis of a new spherical parallel robot with orientation applications, Robotics and Computer-Integrated Manufacturing 37 (2016) 151–161.
[34] M. Karouia, J. M. Hervé, Asymmetrical 3-dof spherical parallel mechanisms, European Journal of Mechanics - A/Solids 24 (1) (2005) 47–57.
[35] G. Wu, S. Caro, J. Wang, Design and transmission analysis of an asymmetrical spherical parallel manipulator, Mechanism and Machine Theory 94 (2015) 119–131.
[36] G. Wu, Parameter–excited instabilities of a 2upu-RUR-RPS spherical parallel manipulator with a driven universal joint, Journal of Mechanical Design 140 (9) (2018) 092303.
[37] I. Tursynbek, A. Niyetkaliyev, A. Shintemirov, Computation of unique kinematic solutions of a spherical parallel manipulator with coaxial input shafts, in: 2019 IEEE 15th International Conference on Automation Science and Engineering (CASE), 2019, pp. 1524–1531.
[38] I. Tursynbek, A. Shintemirov, Infinite torsional motion generation of a spherical parallel manipulator with coaxial input axes, in: 2020 IEEE/ASME International Conference on Advanced Intelligent Mechatronics (AIM), 2020, pp. 1780–1785.
[39] A. Niyetkaliyev, A. Shintemirov, An approach for obtaining unique kinematic solutions of a spherical parallel manipulator, in: 2014 IEEE/ASME International Conference on Advanced Intelligent Mechatronics (AIM), 2014, pp. 1355–1360.
[40] A. Shintemirov, A. Niyetkaliyev, M. Rubagotti, Numerical optimal control of a spherical parallel manipulator based on unique kinematic solutions, IEEE/ASME Transactions on Mechatronics 21 (1) (2016) 98–109.
[41] W. M. Craver, Structural analysis and design of a three degree of freedom robotic shoulder module, Master's thesis, University of Texas, Austin TX (1989).
[42] S. Bai, M. R. Hansen, J. Angeles, A robust forward-displacement analysis of spherical parallel robots, Mechanism and Machine Theory 44 (12) (2009) 2204–2216.
[43] C. M. Gosselin, M. Gagné, A closed-form solution for the direct kinematics of a special class of spherical three-degree-of-freedom parallel manipulators, in: Solid Mechanics and Its Applications, Springer Netherlands, 1995, pp. 231–240.
[44] J.-P. Merlet, Closed-form resolution of the direct kinematics of parallel manipulators using extra sensors data, in: [1993] Proceedings IEEE International Conference on Robotics and Automation, IEEE Comput. Soc. Press.
[45] I. Bonev, J. Ryu, S.-G. Kim, S.-K. Lee, A closed-form solution to the direct kinematics of nearly general parallel manipulators with optimally located three linear extra sensors, IEEE Transactions on Robotics and Automation 17 (2) (2001) 148–156.
[46] H. Sadjadian, H. D. Taghirad, Comparison of different methods for computing the forward kinematics of a redundant parallel manipulator, Journal of Intelligent and Robotic Systems 44 (3) (2005) 225–246.
[47] A. Dumlu, K. Erenturk, Trajectory tracking control for a 3-DOF parallel manipulator using fractional-order $PI^{\lambda}D^{\mu}$ control, IEEE Transactions on Industrial Electronics 61 (7) (2014) 3417–3426.
[48] H. Saafi, M. A. Laribi, S. Zeghloul, Optimal haptic control of a redundant 3-RRR spherical parallel manipulator, in: 2015 IEEE/RSJ International Conference on Intelligent Robots and Systems (IROS), 2015, pp. 2591–2596.
[49] T. Taunyazov, M. Rubagotti, A. Shintemirov, Constrained orientation control of a spherical parallel manipulator via online convex optimization, IEEE/ASME Transactions on Mechatronics 23 (1) (2018) 252–261.
[50] E. Rohmer, S. P. N. Singh, M. Freese, CoppeliaSim (formerly V-REP): a versatile and scalable robot simulation framework, in: Proceedings of The International Conference on Intelligent Robots and Systems (IROS)", 2013, pp. 1321–1326.
[51] I. Tursynbek, A. Shintemirov, Modeling and simulation of spherical parallel manipulators in CoppeliaSim (V-REP) robot simulator software, in: 2020 International Conference Nonlinearity, Information and Robotics (NIR), IEEE, 2020.
[52] S. Bai, M. R. Hansen, Forward kinematics of spherical parallel manipulators with revolute joints, in: Proceedings of the 2008 IEEE/ASME International Conference on Advanced Intelligent Mechatronics (AIM), 2008, pp. 522–527.
[53] D. C. Sorensen, Newton's method with a model trust region modification, SIAM Journal on Numerical Analysis 19 (2) (1982) 409–426.
[54] B. Siciliano, O. Khatib, Springer Handbook of Robotics, Springer-Verlag, Berlin, Heidelberg, 2007.
[55] C. Gosselin, J. Angeles, Singularity analysis of closed-loop kinematic chains, IEEE Transactions on Robotics and Automation 6 (3) (1990) 281–290.
[56] C. M. Gosselin, J. Wang, Singularity loci of a special class of spherical three-degree-of-freedom parallel mechanisms with revolute actuators, The International Journal of Robotics Research 21 (7) (2002) 649–659.
[57] S. Bai, M. Hansen, T. Andersen, Modelling of a special class of spherical parallel manipulators with euler parameters, Robotica 27 (02) (2008) 161–170.
[58] I. A. Bonev, C. Gosselin, Singularity loci of spherical parallel mechanisms, in: Proceedings of the 2005 IEEE International Conference on Robotics and Automation (ICRA 2005), 2005, pp. 295–2962.
[59] C. Gosselin, J. Angeles, A global performance index for the kinematic optimization of robotic manipulators, Journal of Mechanical Design 113 (3) (1991) 220–226.
[60] G. Wu, Kinematics and dynamics of an asymmetrical parallel robotic wrist, Journal of Robotics 2014 (2014) 1–13.
[61] L. J. Puglisi, R. J. Saltaren, H. A. Moreno, P. F. Cárdenas, C. Garcia, R. Aracil, Dimensional synthesis of a spherical parallel manipulator based on the evaluation of global performance indexes, Robotics and Autonomous Systems 60 (8) (2012) 1037–1045.
[62] R. Ranganath, P. S. Nair, T. S. Mruthyunjaya,

A. Ghosal, A force–torque sensor based on a Stewart Platform in a near-singular configuration, Mechanism and Machine Theory 39 (9) (2004) 971–998.

[63] S. Gottschalk, M. C. Lin, D. Manocha, OBBTree: A Hierarchical Structure for Rapid Interference Detection, in: Proceedings of the 23rd annual conference on Computer graphics and interactive techniques - ACM SIGGRAPH, 1996, pp. 171–180.

[64] M. Satoh, Icosahedral grids, in: Atmospheric Circulation Dynamics and General Circulation Models, Springer Berlin Heidelberg, 2013, pp. 636–660.

[65] R. K. Mobley, Gears and gearboxes, in: Plant Engineer's Handbook, Elsevier, 2001, pp. 629–637.

Appendix A. Examples of sampled rotational motions

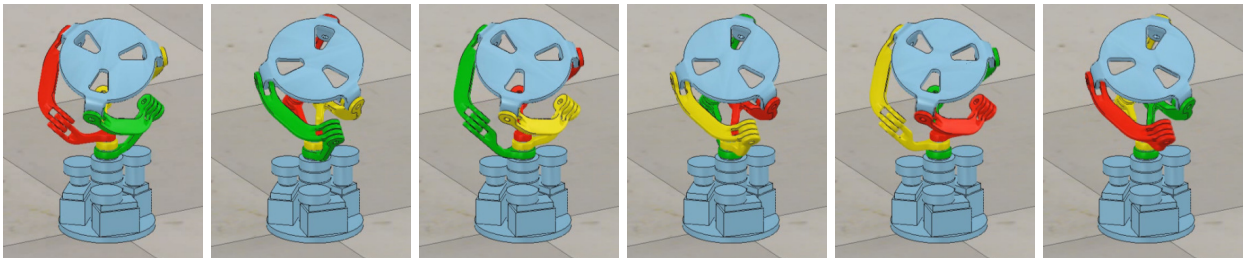

(a) $\sigma = 0°$ (b) $\sigma = 60°$ (c) $\sigma = 120°$ (d) $\sigma = 180°$ (e) $\sigma = 240°$ (f) $\sigma = 300°$

Figure A.11: Rotational instances of the simulated coaxial SPM model about unit vector $\mathbf{n} = [-0.274, -0.555, 0.786]^T$.

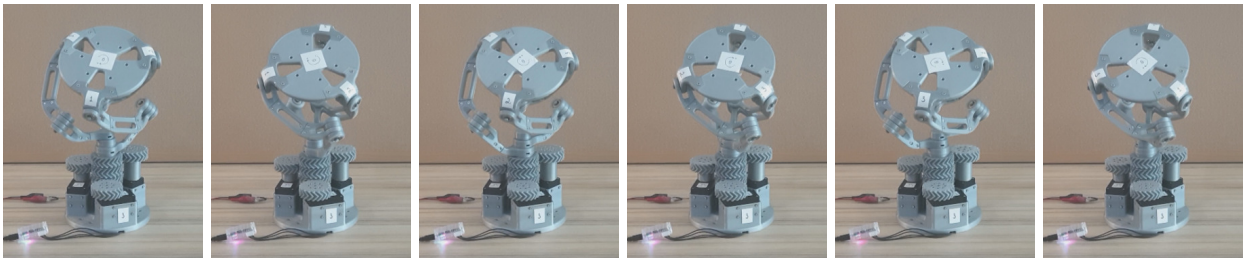

(a) $\sigma = 0°$ (b) $\sigma = 60°$ (c) $\sigma = 120°$ (d) $\sigma = 180°$ (e) $\sigma = 240°$ (f) $\sigma = 300°$

Figure A.12: Rotational instances of the experimental coaxial SPM prototype about unit vector $\mathbf{n} = [-0.274, -0.555, 0.786]^T$.

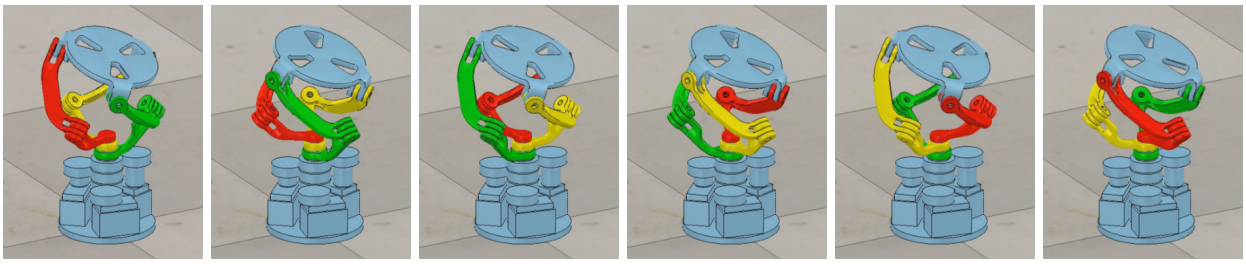

(a) $\sigma = 0°$ (b) $\sigma = 60°$ (c) $\sigma = 120°$ (d) $\sigma = 180°$ (e) $\sigma = 240°$ (f) $\sigma = 300°$

Figure A.13: Rotational instances of the simulated coaxial SPM model about unit vector $\mathbf{n} = [0.165, -0.326, 0.931]^T$.

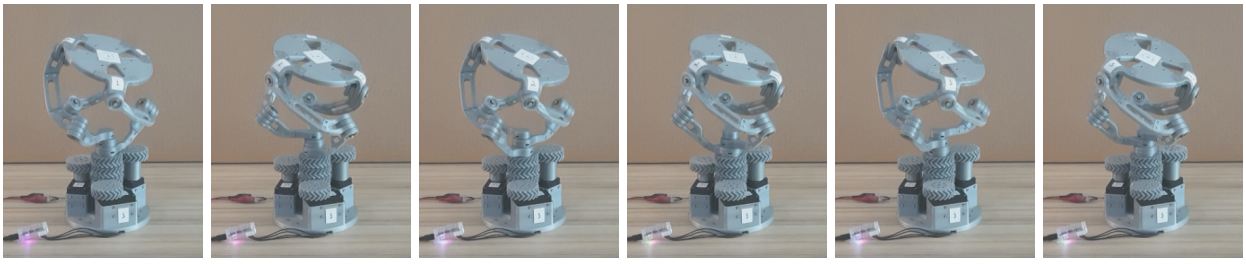

(a) $\sigma = 0°$ (b) $\sigma = 60°$ (c) $\sigma = 120°$ (d) $\sigma = 180°$ (e) $\sigma = 240°$ (f) $\sigma = 300°$

Figure A.14: Rotational instances of the experimental coaxial SPM prototype about unit vector $\mathbf{n} = [0.165, -0.326, 0.931]^T$.

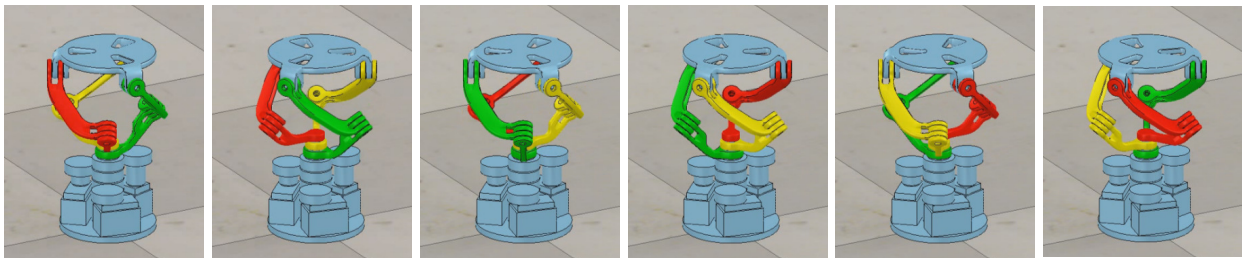

(a) $\sigma = 0°$ (b) $\sigma = 60°$ (c) $\sigma = 120°$ (d) $\sigma = 180°$ (e) $\sigma = 240°$ (f) $\sigma = 300°$

Figure A.15: Rotational instances of the simulated coaxial SPM model about unit vector $\mathbf{n} = [0, 0, 1]^T$.

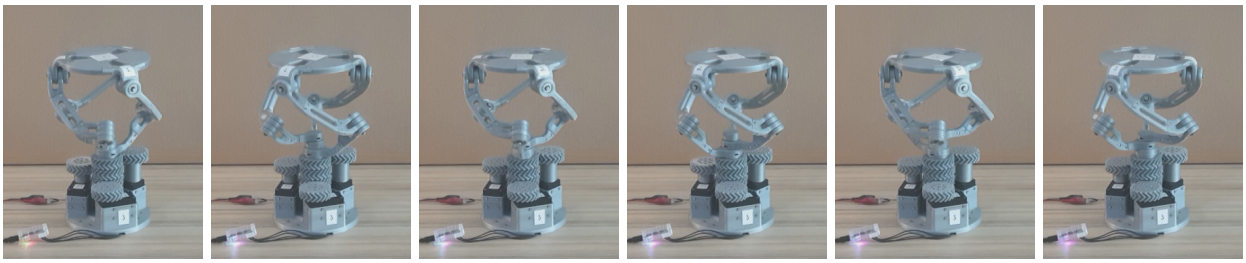

(a) $\sigma = 0°$ (b) $\sigma = 60°$ (c) $\sigma = 120°$ (d) $\sigma = 180°$ (e) $\sigma = 240°$ (f) $\sigma = 300°$

Figure A.16: Rotational instances of the experimental coaxial SPM prototype about unit vector $\mathbf{n} = [0, 0, 1]^T$.